hep-ph/9508350
HD-THEP-95-36

SMALL SCALE STRUCTURE PREDICTIONS FROM DISCRETE SYMMETRY BREAKING – EARLY QUASAR FORMATION

Smaragda Lola

Institut für Theoretische Physik, Univerisität Heidelberg,
Philosophenweg 16, 69120 Heidelberg, Germany

Abstract

We discuss the local density fluctuations which arise due to the topological defects that appear after the phase transition of light pseudo-Goldstone bosons. It has been found that in a post-inflationary universe the fluctuations of these defects at large scales may have led to galaxy formation, while being consistent with the measurements of the cosmic microwave background radiation. Here we show that, at the local level, the fluctuations may be sufficiently large to lead to the production of smaller structures (ie quasars) with the observed distribution, which peaks at $z = 2$ and drops rapidly for higher redshifts. Moreover it may be possible that a limited number of quasars are produced at redshifts of order 10, much earlier than what hot and cold dark matter scenarios predict. Although in this letter we work in the parameter space which is optimal for the generation of large scale structure as well, these features are generic for a wide class of domain wall models.

1 Introduction

Over the recent years, there has been a growing interest in the origin of the observed large scale structure of the universe, due to the data coming from COBE [1] and from the extensive IRAS survey [2]. One of the most important conclusions of both measurements is that the standard cold or hot dark matter (CDM or HDM) scenarios with a Harrison-Zeldovich spectrum of primeval fluctuations, fail to account on their own for the complete spectrum of energy density fluctuations. In the case of cold dark matter, which has been considered as the most promising solution, the scale invariance of the spectrum results in a discrepancy: either the data fits well with the theory at large scales and then the predicted structure at smaller scales is unacceptably large, or the data is normalised to agree with the observations at small scales and then there is not enough power at the long wavelength components of the theoretical spectrum.

In several particle physics models, there has been a lot of effort to provide additional sources of fluctuations at large scales [3] In one of these attempts, we have applied percolation theory in order to perform a detailed analysis of the density perturbations that are to be expected from the domain walls forming during the phase transition of very light fields [4]. This statistical method, which has first been introduced in the study of domain wall distributions in the universe by Lalak, Ovrut and Thomas [5], allowed us to formulate a picture of the spatial distribution of the overdensities in a post-inflationary universe. We found that the domain walls may act as seeds of structure formation and enhance the standard cold dark matter spectrum, in such a way as to account for the whole range of observations of IRAS and COBE and still be consistent with the measurements of the cosmic microwave background radiation. This occurs, provided that one of the minima of the potential of the scalar field is favoured, and in [4, 6] it has been demonstrated why this is true after inflation has taken place[1].

Here, we will extend the analysis in the small scale distribution of matter. In these lines, it is of particular interest to find at what redshift the first structures are expected to form and how large is the amount of mass that has become non-linear at that time. The objects with the higher observed redshift, z_q, are quasars. In the recent years the limits on z_q have increased and for the more distant quasar that has been seen up to now, $z_q \sim 5$ [8]. The standard cold dark matter picture can account for early quasar formation with difficulty and the situation will become worse if new, more distant objects are seen at even higher redshifts. For this reason, one would like to see whether domain walls may trigger sufficiently large density fluctuations which lead to quasar production at

[1] In the case that both minima appear with the same probability, horizon size domain walls which would result to unacceptably large fluctuations in the cosmic microwave background radiation arise [7].

early times. This was found to be the case in [9], where models with unstable domain walls have been considered. We showed that, due to a small degeneracy in the minima of the potential of a pseudo-Goldstone boson, which may arise in string models, there exists a critical horizon scale at which the true vacuum dominates and all walls disappear. However, when the wall bubbles that surround a region of true vacuum expand, rapid collisions and domain wall annihilation occurs, resulting in large local overdensities, which can host quasars. Redshifts as large as 10 were predicted, which are much larger than those expected in CDM models.

In schemes with stable walls, where the field may roll to the minima of its potential with different probability, overdensities at the local level are also to be expected. Using percolation theory, it is possible to examine not only at what red-shifts the mass in the non-linear regime becomes sufficient for the formation of stellar objects, but also what is their spatial distribution. The data indicates that at high and low redshifts there exists a decrease in the distribution of quasars, the peak being at $z \approx 2$. In this work, we will attempt to gain some insight, as to why this occurs.

2 Domain walls in the percolation theory picture

Domain walls are associated with discrete symmetries, which arise commonly in many particle physics models, after the explicit breaking of a continuous symmetry [10]. The resulting potential of the pseudo-Goldstone bosons is of the form

$$V = V_0 \left[\cos\left(\frac{\phi}{v}\right) + 1 \right] \tag{1}$$

and obeys the discrete symmetry $\phi \rightarrow \phi + 2\pi n v$, $n = 1, 2...$ The equation of motion corresponding to the above potential, admits domain wall solutions that interpolate between two adjacent vacua [11]. The width of the walls, Δ, is given by

$$\Delta = \frac{v}{\sqrt{V_0}} = m^{-1} \tag{2}$$

m being the mass of ϕ evaluated at any minimum. The surface energy density of the wall is

$$\sigma = \int_{-\infty}^{+\infty} 2V_0 \left[\cos\left(\frac{\phi}{v}\right) + 1 \right] dz = 8\, v^2 m \tag{3}$$

The space distribution of the domain walls is found by partitioning the three-dimensional space into cubic lattice sites with lattice spacing Λ [5]. In this letter, as in [4], we work with a system that has two minima. It is assumed that at each

lattice site the physical system can be in one of the two vacua, denoted by $(+)$ and $(-)$ respectively. The probability that a lattice site is in the $(+)$ vacuum is denoted by p, $0 \leq p \leq 1$, while the probability that a lattice site is in the $(-)$ vacuum is $q = 1 - p$. Provided there is no correlation between the vacuum structures at any two different lattice sites, it is possible to calculate the spatial distribution of the two vacua and, hence, the spatial distribution of domain walls, by applying three-dimensional percolation theory [12]. It has been shown that for $p < p_c$, where $p_c = 0.311$ is the critical probability for a cubic lattice in three dimensions, the $(-)$ vacua lie predominantly in a large percolating cluster (since necessarily $q > p_c$), while the $(+)$ vacua are in finite s-clusters. Here, s denotes the number of nearest neighbour lattice sites that are occupied by $(+)$. Moreover, it was recently found that the scaling behaviour of the percolating cluster is not persistent until p reaches the value $p = 1/2$ [6]. This indicates that for a large range of probabilities only finite wall bubbles are present. On a given lattice, the number of s-clusters falls rather quickly with growing s. Indeed, the probability per lattice site that a given lattice site is an element of an s-cluster, $n_s(p)$, (which is given by the ratio of the total number of s-clusters, N_s, over the total number of lattice sites, N) is

$$n_s(p) = 0.0501 s^{-\tau} \exp\left\{-0.6299 \left(\frac{p - p_c}{p_c}\right) s^{\sigma} \left[\left(\frac{p - p_c}{p}\right) s^{\sigma} + 1.6679\right]\right\} \qquad (4)$$

where $\tau = 2.17$ and $\sigma = 0.48$ [5]. Since for a given lattice there exists an upper statistical cut-off on the size of observable clusters, no unacceptable fluctuations of the cosmic microwave background radiation due to domain wall bubbles are generated [4].

The mean radius of a wall bubble at a specific redshift is well characterized by the average radius of gyration, $R_s(p)$, of an s-cluster. This quantity (for $p < p_c$ and $s > s_\xi$) is found to be

$$R_s(p) = f_s(p)\Lambda \equiv 0.702(p_c - p)^{0.322} s^{0.55} \Lambda \qquad (5)$$

where

$$s_\xi = \left(\frac{0.311}{|p - 0.311|}\right)^{2.08} \qquad (6)$$

Initially, R_s is larger than the horizon. However, the horizon radius grows faster than that of the bubble (whose radius just grows linearly with the expansion), and thus at some redshift $z_a(s)$ the bubble comes within the horizon. At this stage the bubble shrinks under its surface tension, undergoes a few cycles of oscillations, and finally looses its energy in the form of scalar waves [13]. The energy stored in the domain wall is

$$E_s = f t_s \sigma \Lambda^2, \quad t_s = s\left(\frac{1 - p}{p}\right) \qquad (7)$$

where t_s is the average surface area of an s-cluster. The parameter f is $1 \leq f \leq 6$ and here we use the moderate value $f = 3$. Due to the expansion of the universe, the lattice spacing Λ is a function of the redshift z. The redshift when the wall bubbles shrink, $z_a(s)$, is taken to be the redshift when an s-cluster enters the horizon. The overdensities that are expected to arise after the bubbles shrink are calculated in a subsequent section. However, even at this stage, it is possible to predict the qualitative picture that arises and to see its relevance for quasar formation.

3 Quasar production and spectrum

Quasars are high-redshift active galaxies, with a very energetic central source of energy, which may not be coming from nuclear fusion. The most popular scheme is that quasars are powered by the accretion of matter in a supermassive black hole ($M_h \approx 10^8 M_\odot$) in the center of a host galaxy [14]. Then, before any quasar activity can begin, some galaxies must have formed and virialised at redshifts higher than that of the actual quasar and subsequently evolved to the stage of developing a massive black hole. This indicates that the very existence of quasars implies that non-linear structures must have appeared at redshifts higher than 5.

Studies of the space distribution of quasars show that their number density exhibits a peak at a redshift $z \approx 2$; for smaller redshifts the observed abundance of quasars decreases. The space density of quasars with redshift $z < 2$ has been measured to be roughly 10^{-5} Mpc^{-3}. For redshifts $z > 2$ there is also a decrease of the number of quasars as the redshift goes up, except for the very bright ones. This decrease however is gradual, rather than a steep cut-off. It is also possible to estimate the mass that ought to collapse at a redshift z_q, in order to lead to quasar production at a later time. For example, for a quasar with a redshift 4 it is found that the minimal collapsing mass should be at least $O(10^{12} M_\odot)$, and this value can be even larger.

However, such a picture for the local fluctuations is exactly what we would expect from percolation theory. The basic points to note are that:

• the larger domain wall bubbles enter the horizon and shrink under surface tension later than the smaller ones. Since

• wall-driven fluctuations redshift slower than radiation or matter,

• the local fluctuations that involve larger bubbles may become non-linear at higher redshifts. On the other hand, percolation theory predicts that

• the number of lattice sites n_s decreases exponentially with s, thus the number density of bubbles decreases with their size.

The combined effect is that *non-linear fluctuations at very high redshifts become rare*. As for the decrease in the number of quasars as the redshift drops below 2 it can also be explained. This is because

• For larger wall bubbles, the amount of mass in the non-linear regime is larger. It is possible therefore that at $z = 2$ we approach a critical mass scale which is slightly higher from the minimum value that we need in order for quasar formation to proceed. Then, at that redshift the quasar density will be expected to be maximal, while at lower redshifts the number of objects will decrease.

• Finally, for the brighter quasars more mass is required in the non-linear regime, therefore they will appear only at high redshifts.

Note that these features are generic and lead to the same qualitative picture for different regions of the parameter space and in particular for different choices of the mass of the field, m, which sets the time-scale of the transition[2].

4 Local density fluctuations

While the qualitative behaviour that has been discussed is generic, in order to gain a better understanding, we will calculate the local density fluctuations in a specific scheme. Here, we will chose to work with the same parameter space which in [4] was found to lead to the best agreement with the data at large scales.

In [4], in order to compare the wall driven fluctuations with the ones observed at the large scales, the energy density E_s had been averaged over the mean distance between s-clusters at z_a. The Fourier analysis of a quasi-periodic matter distribution shows that the amplitude of the Fourier coefficients is peaked in the momentum space around a set of discrete points corresponding to the wavelengths $\lambda = \infty, d, d/2, ..., R$, where d is the mean distance between seeds and R is the typical radius of the overdensity produced by the accretion of matter onto the seed in question. In the scenario described in [4] it has been assumed that $R \approx d$ (that is a big amount of the overdensity detached by each cluster is dispersed over a region not much smaller than d). This is a reasonable assumption as the seeds considered in [4] are produced in the radiation dominated epoch, and one can argue that the accretion is not very effective at that time. However, we do not know how large R really is. One may expect that the larger clusters, which *enter the horizon at a much later stage*, may drive collapse more efficiently and leave behind more compact overdensities whose radii are smaller than d and as small as R_s. We think that this is a reasonable assumption, for the following reasons:

[2] Only when the length scale m^{-1} comes within the horizon, can the field roll towards its minima [4] .

• Although the phase transition occurs deep in the radiation dominance, the larger clusters enter the horizon at the very end of the radiation era. At that time matter has already started to slow down significantly, therefore part of it may accrete around the wall just before the latter collapses. In this case we can define an "efficiency parameter", γ_ℓ, which scales with the redshift. This parameter should become unity in matter dominance (where subsequently the fluctuations grow proportionally to the redshift), while the earlier the wall bubble enters the horizon, as compared to the beginning of the matter dominance era, the smaller the efficiency parameter becomes. We come back to this point in the quantitative examples that will be presented.

• The larger walls store more energy, therefore they drive more efficient collapse.

• In addition, although in [4] we have prefered to work with non-interacting light scalar fields, as they are out of equilibrium and their mass is naturally in the correct range for structure formation, it is also possible that some *interaction* between the light fields and ordinary matter is present. In [15] it has been shown that very light pseudo-Goldstone bosons may give rise to long range forces. In the case that an interaction exists, localized density fluctuations due to domain walls may appear [16]. If this interaction is very weak, it still will not be sufficient to change the out-of-equilibrium property of the system, which has the general behaviour that we have described in [4]. Nevertheless, even a very soft interaction can result in amplifying the local energy dissipation mechanism in comparison to the situation where only gravity is present in the theory. As we are going to see below, an efficiency for matter accretion as low as $\approx 10\%$, around collapsing domain walls which enter the horizon at the end of the radiation era, is sufficient to support the picture we propose.

• Finally, while here we chose to work with the parameter space that was found in [4] to be optimal for the creation of large scale structure due to a single phase transition, it would be possible to relax this condition. In such a case, we can assume that the mass of the pseudo-Goldstone boson, m, can be smaller, such that the larger walls which give rise to the local density fluctuations that subsequently will host quasars, enter the horizon and dissipate their energy in the matter dominance era. In [4] m was fixed by demanding that the peak of the density fluctuations as a function of the scale occurs at ≈ 30 Mpc, as observations indicate. What happens when m is smaller? The first point to make is that the density fluctuations at large scales will decrease, since the fluctuations now have less time to grow (here we should note that for large scale structure, the relevant fluctuations are of super-horizon size and grow as the square of the red-shift during the radiation era [17], while the local fluctuations practically grow only in matter dominance). The larger domain walls may now enter the horizon deep inside matter dominance and the resulting local density fluctuations are amplified. As we have pointed out, the basic features which determine the quasar distribu-

tion *are generic* and give rise to a similar qualitative behaviour if a smaller m is chosen.

The picture we have therefore is that overdensities at scales larger than the respective R_s, as well as the local overdensities which do not become nonlinear early enough, form a kind of a diffusive background on top of which some overdensities at the local level may form gravitationally bound structures, for instance galaxies hosting quasars. In what follows we will try to estimate the expected spectrum of such structures. For this, we need to calculate the overdensity at a local level and the scale over which the averaging is done is the one that may provide mass greater than this of a quasar, in the non-linear region $\delta\rho/\rho \geq 1$. The smallest possible distance over which we may average (leading to the larger local fluctuations) is the horizon at a redshift z_a, $R_{H_a} \equiv R_H(z_a)$.

Let us now pass to specific formulas: The redshift z_a is obtained by equating the mean radius of gyration for an s-cluster, to the horizon at that redshift. We find that

$$1 + z_a = \frac{1 + z_t}{\alpha f_s(p)} \tag{8}$$

with

$$(1 + z_t)^2 = \frac{R_{H_0}}{R_H(z_t)}(1 + z_d)^{1/2} \tag{9}$$

where z_d is the redshift when matter domination begins and $R_{H_0} = 6000$ Mpc is the horizon size today[3]. The factor $\alpha \equiv H(z_t)/H(z_f)$, where z_t is the redshift where the field starts rolling down the potential towards one of its minima, and $z_f < z_t$ denotes the time at which the system actually settles in one of the vacua, after a period of oscillations [4]. The above formulas hold for $z_a \geq z_d$.

Assuming that the mean total energy density is equal to the critical density, we may express the critical energy density at z_a in terms of the present day critical density ρ_0 as

$$\rho_c(z_a) = \rho_0 \frac{(1 + z_a)^4}{1 + z_d} \tag{10}$$

The local energy density perturbation due to an s-cluster with diameter R_{H_a} at $z_a(s)$ is

$$\left.\frac{\delta\rho}{\rho}\right|_a \equiv \left.\frac{\delta\rho}{\rho}\right|_{local}(z_a) = \frac{6\, f\, \sigma\, (1-p)\, s\, \Lambda_a^2}{p\, \rho_c(z_a)\, \pi\, R_{H_a}^3} \tag{11}$$

where

$$\Lambda_a \equiv \Lambda(z_a) = \frac{\alpha}{m}\frac{1 + z_t}{1 + z_a} \tag{12}$$

[3]Throughout the calculation we are going to assume that the reduced Hubble constant h is unity (that is the Hubble constant today is $H_0 = 100\,\mathrm{km\,s^{-1}\,Mpc^{-1}}$), for simplicity of presentation. A different value of h does not alter the picture we have. In this case, the input model parameters that are needed to fit the large scale data, which are the same that we use here for small scale predictions, are shifted to σh^2 and vh, as explained in [4] .

is the lattice spacing at z_a[4] and

$$R_{H_a} = \frac{1}{m} \left(\frac{1+z_t}{1+z_a}\right)^2 \tag{13}$$

The local fluctuations are (in contrast to the fluctuations that give rise to the large scale structure) always sub-horizon and therefore grow logarithmically with the redshift during radiation dominance and linearly during matter dominance. Then the redshift z_q at which the fluctuations become non-linear is given by

$$1 + z_q = \gamma_\ell \left.\frac{\delta\rho}{\rho}\right|_a (1+z_d)\left(1 + 2\log\frac{1+z_a}{1+z_d}\right) \tag{14}$$

The factor $\gamma_\ell < 1$ which appears in (11), has been added in order to take into account that for the parameter space where we work, at the end of the radiation dominance only a part of the overdensities that are produced by the wall bags will remain localized.

The total amount of mass in the non-linear region at z_q, M_q, in terms of solar masses $M_\odot$, is given by

$$M_q = \frac{\pi L_q^3}{6M_\odot}\rho_c(1+z_q)^3 \tag{15}$$

where the scale of the perturbation at z_q is

$$L_q = R_{H_a}\frac{1+z_a}{1+z_q} \tag{16}$$

and $M_\odot$ is the solar mass. Finally, we can identify the space distribution of the local fluctuations. The average distance between s-clusters at a redshift z is

$$d(z) = \left(\frac{V(z)}{V(z)n_s}\right)^{1/3}\Lambda(z) \tag{17}$$

thus today

$$d(z=0) = \frac{1}{n_s^{1/3}}\frac{a}{m}(1+z_t) \tag{18}$$

5 Numerical analysis

In [4] we have found that large scale structure may form as a result of the global density fluctuations (fluctuations averaged on scales d), and some indicative combinations for $\alpha = 10$ appear on Table 1. Here we want to use the same set of parameters to examine the local overdensities of the model. However, in [4] we

[4] $\Lambda(z_t) \equiv a/m$ [5, 4].

had also introduced a parameter γ_s (to account for the fact that before a wall bag disappears, it may stay around sufficiently long to cause the collapse of amounts of matter). This coefficient may not be determined precisely without a more detailed analysis in the framework of the spherical collapse model. In [4] we took the value $\gamma_s = 10$, however if this parameter is of order unity, the only modification in our results would be that we need a higher value of v to fit the IRAS and COBE data. The model parameters that lead to solutions, for $\gamma_s = 1$, are given in Table 2.

In the present work we take γ_s at its minimum value and on top of that we have introduced γ_ℓ, to account for the fact that the wall bubbles that we consider appear in the end of the radiation dominance (if $\gamma_s > 1$, even larger efficiency in the accretion of the local overdensities would be expected). To see whether it is possible to get the correct qualitative behaviour for the distribution of local overdensities, we consider the following possibilities:

(i) γ_ℓ $O(0.2)$. Such a constant factor (especially shifted towards larger values) may be expected if some soft interactions are present.

(ii) γ_ℓ $O(0.1)$.

(iii) In the absence of interactions, the most realistic approach is to take into account that larger bubbles lead to a more efficient energy dissipation, since they enter the horizon nearer the matter dominance era, where the overdensities grow linearly with the redshift. For this reason we set $\gamma_\ell = (1 + z_d)/(1 + z_a)$. For $z_a \approx z_d$ the efficiency parameter is unity, since we are in matter dominance, while the higher z_a is, the smaller the parameter becomes.

Using the model parameters of Table 2, we have calculated the local density fluctuations as well as their space distribution, the redshift z_q where the fluctuations become non-linear and the amount of mass that is involved in the non-linear regime. The results appear on Tables 3,4 and 5 for the three choices of input parameters respectively. These tables indicate that for all three choices, the amount of mass in the non-linear region can be sufficiently large to allow for early quasar formation. Moreover, we reproduce qualitatively the observed space distribution of quasars, at redshifts $z \geq 2$, that is quasars at larger redshifts appear with larger space separation. We also observe that the mass in the non-linear regime reduces with the red-shift, indicating that after a certain redshift the total available amount of mass will be near the lower limit that we need for quasar production. We find that for this to occur at $z = 2$, the mass should be $O(10^{13}\ M_\odot)$. Concerning the scale of the perturbation, in all cases is found to be $O(\mathrm{Mpc})$. We also see that the number of quasars at a specific redshift is sensitive to the parameter p. Indeed, for p = 0.11 we find that $s = 50$ leads to one quasar every 1614 Mpc, while for p =0.15 the distance is 461 Mpc.

The number of quasars and the total mass in the non-linear regime, as functions

of the red-shift, for the three cases of Table 2, are given in figures 1-6. We see that the qualitative behaviour is in agreement with observations and that even with the rough approximations that we have made, the quantitative agreement is also good.

6 Conclusions

To summarise, we have looked at the local density fluctuations generated by domain walls after the phase transition of light pseudo-Goldstone bosons. In particular, we have analyzed the expected density perturbations and their spatial distribution, as well as the redshifts at which they become non-linear. We have found that, complementary to the generation of the observed large scale structure, the same overdensities may lead at the local level to an early appearance of non-linear fluctuations which may result to early quasar production. The scale of the overdensities is naturally of the correct order of magnitude. Concerning the spectrum of these objects, we show that quasars are expected to appear with larger space separation as the redshift increases, in consistency with observations. A decrease to the number of objects as the redshift falls below a critical value is also predicted. The total amount of mass that is involved in this non-linear process is from $10^{12} - 10^{14} M_{\odot}$, which is interesting, given that $10^{12} M_{\odot}$ is the minimal possible value for an overdensity to evolve to a galaxy that may host a quasar.

Acknowledgment

I am grateful to Z. Lalak, B. Ovrut and G. G. Ross for many enlightening discussions on the subject.

References

[1] G. F. Smoot et al., Astrophys. J. Lett. 396 (1992), L1.

[2] M. Rowan-Robinson et al., Mon. Not. R. Astr. Soc. 247 (1990) 1; W. Saunders et al., Nature 349 (1991) 32; N. Kaiser et al., Mon. Not. R. Astr. Soc. 252 (1991) 1; W. Saunders, M. Rowan-Robinson and A. Lawrence, Mon. Not. R. Astr. Soc. 258 (1992) 134;

[3] C. T. Hill, D. N. Schramm and J. N. Fry, Comments Nucl. Part. Physics 19 (1989) 25; W. Press, B. Ryden and D. Spergel, Phys. Rev. Lett. 64 (1990) 1084 .

[4] Z. Lalak, S. Lola, B. Ovrut and G. G. Ross, Nucl. Phys. B434 (1995) 675.

[5] Z. Lalak and B. A. Ovrut, Phys. Rev. Lett. 71 (1993) 951; Z. Lalak, B. A. Ovrut and S. Thomas, Phys. Rev. D51 (1995) 5456.

[6] D. Coulson, Z. Lalak and B. Ovrut, hep-ph/9508226.

[7] W. Press, B. Ryden, and D. Spergel, Ap. J. 347 (1989) 590; L. Kawano, Phys. Rev. D41 (1990) 1013.

[8] D. P. Schneider, M. Schmidt and J. E. Gunn, Ap. J. 98 (1989) 1951.

[9] S. Lola and G. G. Ross, Nucl. Phys. B406 (1993), 452.

[10] C. T. Hill and G. G. Ross, Phys. Lett. B205 (1988) 125; C. T. Hill and G. G. Ross, Nucl. Phys. B311 (1988) 253; J. A. Casas and G. G. Ross, Phys. Lett. B198 (1987) 461.

[11] For a review on domain walls, see A. Vilenkin, Phys. Rept. 121 (1985) 263 and references therein.

[12] M. F. Sykes, D. S. Gaunt and Maureen Glen, J. Phys. A: Math. Gen. Vol. 9, No. 10 (1976); A. Flammang Z. Physik B28 (1977) 47.

[13] L. M. Widrow, Phys. Rev. D40 (1989) 1002.

[14] For a review on quasars see T. Padmanabhan, *Structure formation in the universe*, Cambridge University Press, 1993.

[15] D. Chang, R. N. Mohapatra and S. Nussinov, Phys. Rev. Lett. 55 (1985) 2835.

[16] A. Massarotti, Phys. Rev. D43 (1991) 346.

[17] For a review of density fluctuations see E. Kolb and M. Turner, *The Early Universe*, Addison-Wesley Publishing Company, 1990, and references therein.

Table Captions

Table 1. Model parameters generating the observed large scale structure that were presented in [4] (where amplification of the fluctuations due to matter accretion in the wall before the later collapses were considered).

Table 2. Model parameters generating the observed large scale structure for minimal accretion of matter in the wall before the later collapses. The only change from table 1 is in the parameter v.

Table 3. Astrophysical parameters of the quasars for case 1 of table 2. The redshifts z_{q_1}, z_{q_2}, z_{q_3} stand for the three possibilities for the efficiency parameter, $\gamma_\ell = 0.2$, 0.1 and $(1+z_d)/(1+z_a)$ respectively. In this table as well as in the following ones we stop the calculation as soon as d grows beyond the horizon today.

Table 4. Astrophysical parameters of the quasars for case 2 of table 2.

Table 5. Astrophysical parameters of the quasars for case 3 of table 2.

Figure Captions

Figure 1. The number of quasars as a function of the redshift, for $\gamma_\ell = 0.2$. The symbols $+$, $*$ and $\times$ correspond to the three cases of Table 2 respectively. The notation is the same in the rest of the figures as well.

Figure 2. The mass in the non-linear regime as a function of the redshift, for $\gamma_\ell = 0.2$.

Figure 3. The number of quasars as a function of the redshift, for $\gamma_\ell = 0.1$.

Figure 4. The mass in the non-linear regime as a function of the redshift, for $\gamma_\ell = 0.1$.

Figure 5. The number of quasars as a function of the redshift, for $\gamma_\ell = (1+z_d)/(1+z_a)$.

Figure 6. The mass in the non-linear regime as a function of the redshift, for $\gamma_\ell = (1+z_d)/(1+z_a)$.

p	m (GeV)	v (GeV)	s_ξ
0.11	3×10^{-32}	6.3×10^{13}	2.48
0.13	5×10^{-32}	6.3×10^{13}	3.08
0.15	4.5×10^{-32}	7.1×10^{13}	3.93

Table 1

p	m (GeV)	v (GeV)	s_ξ
0.11	3×10^{-32}	2×10^{14}	2.48
0.13	5×10^{-32}	2×10^{14}	3.08
0.15	4.5×10^{-32}	2.24×10^{14}	3.93

Table 2

s	z_a	z_{q_1}	z_{q_2}	z_{q_3}	M_q (in $M_\odot$)	d (Mpc)
5	1.6×10^5	0.4	–	–	6.6×10^{12}	29
10	1.1×10^5	1.6	0.3	0.2	2.1×10^{13}	58
15	8.9×10^4	2.6	0.8	1.0	4.1×10^{13}	99
20	7.6×10^4	3.5	1.2	1.9	6.5×10^{13}	157
25	6.7×10^4	4.3	1.6	2.9	9.4×10^{13}	240
30	6.1×10^4	5.1	2.0	4.0	1.3×10^{14}	360
40	5.2×10^4	6.6	2.8	6.3	2.1×10^{14}	774
50	4.6×10^4	8.0	3.5	8.7	3.0×10^{14}	1614
60	4.2×10^4	9.2	4.1	11.2	4.0×10^{14}	3294

Table 3

s	z_a	z_{q_1}	z_{q_2}	z_{q_3}	M_q (in $M_\odot$)	d (Mpc)
5	2.2×10^5	0.3	–	–	2.8×10^{12}	22
10	1.5×10^5	1.3	0.2	–	8.9×10^{12}	42
15	1.2×10^5	2.2	0.6	0.4	1.7×10^{13}	67
20	1.0×10^5	3.1	1.1	1.0	2.7×10^{13}	100
25	9.0×10^4	4.0	1.5	1.7	4.0×10^{13}	144
30	8.1×10^4	4.7	1.8	2.5	5.4×10^{13}	202
40	6.9×10^4	6.2	2.6	4.1	8.6×10^{13}	386
50	6.1×10^4	7.4	3.2	5.9	1.2×10^{14}	713
60	5.5×10^4	8.7	3.8	7.7	1.7×10^{14}	1288
70	5.1×10^4	9.9	4.4	9.6	2.2×10^{14}	2294
80	4.7×10^4	11.0	5.0	11.6	2.7×10^{14}	4046

Table 4

s	z_a	z_{q_1}	z_{q_2}	z_{q_3}	M_q (in $M_\odot$)	d (Mpc)
5	2.1×10^5	0.4	–	–	2.9×10^{12}	23
10	1.5×10^5	1.5	0.2	–	9.1×10^{12}	41
15	1.2×10^5	2.5	0.7	0.5	1.8×10^{13}	62
20	1.0×10^5	3.4	1.2	1.2	2.9×10^{13}	89
25	8.8×10^4	4.2	1.6	1.9	4.1×10^{13}	121
30	8.0×10^4	5.0	2.0	2.8	5.6×10^{13}	162
40	6.8×10^4	6.6	2.8	4.5	9.0×10^{13}	278
50	6.0×10^4	8.0	3.5	6.4	1.3×10^{14}	461
60	5.5×10^4	9.3	4.1	8.4	1.8×10^{14}	748
70	5.0×10^4	10.6	4.8	10.5	2.3×10^{14}	1196
80	4.7×10^4	11.8	5.4	12.7	2.8×10^{14}	1893
90	4.4×10^4	12.9	5.9	14.9	3.4×10^{14}	2972
100	4.1×10^4	14.0	6.5	17.0	4.1×10^{14}	4636

Table 5

Figure 1

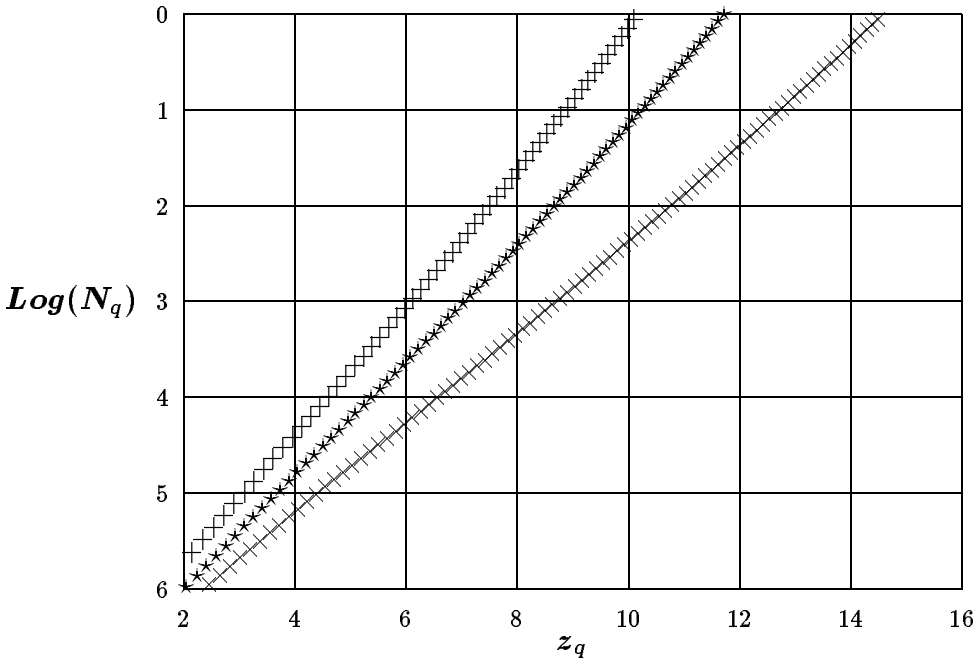

Figure 2

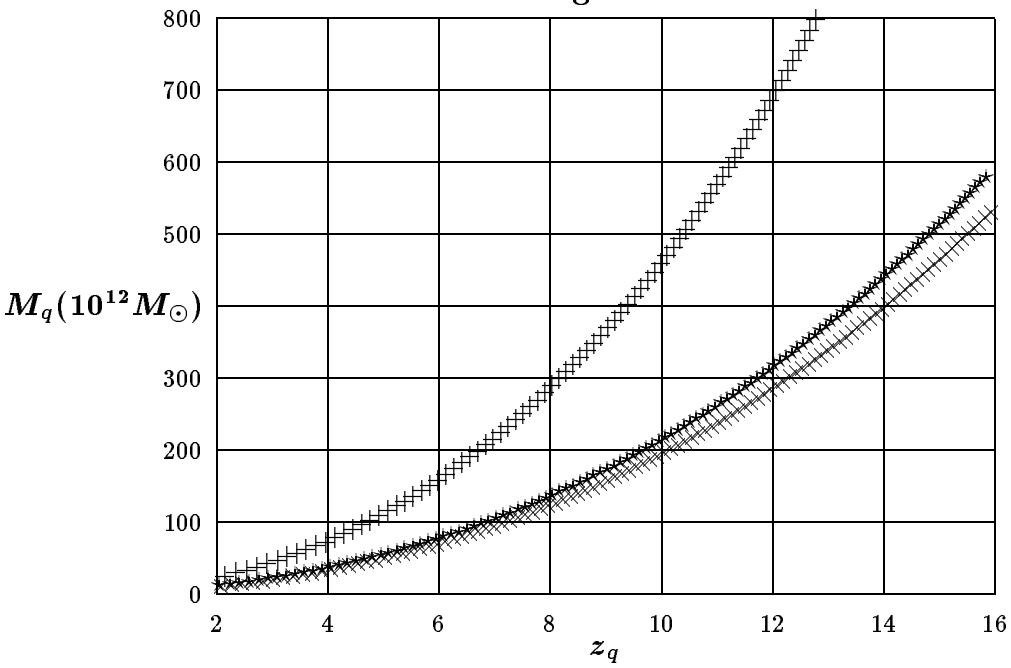

Figure 3

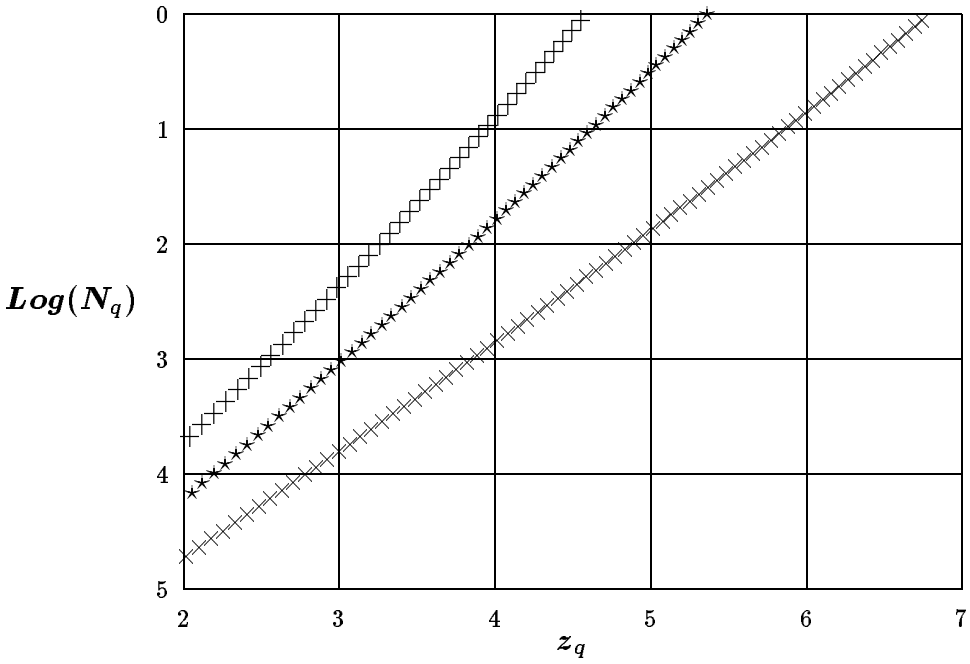

Figure 4

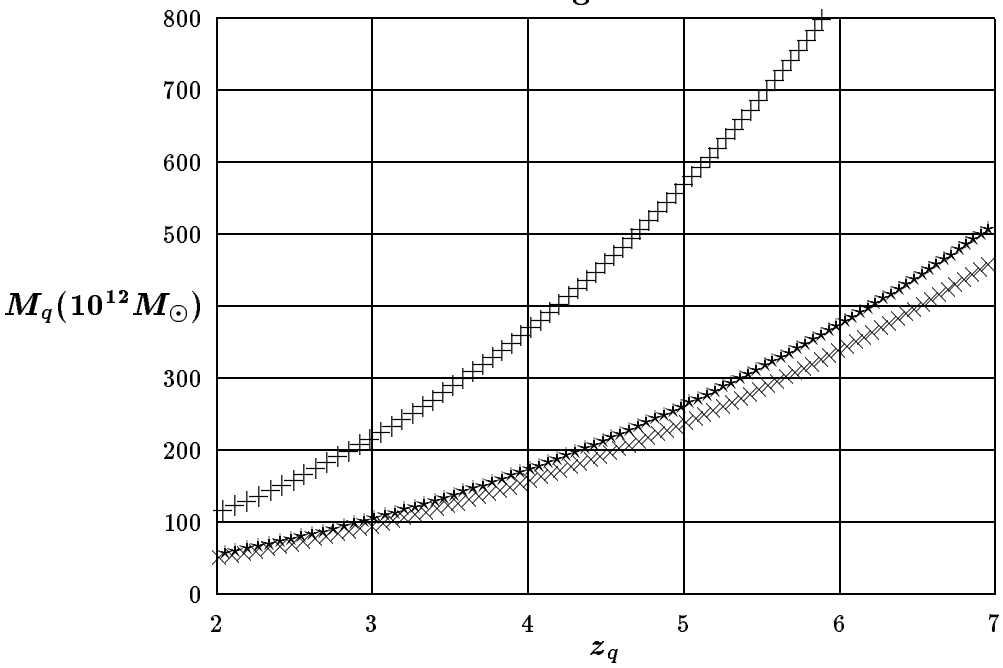

Figure 5

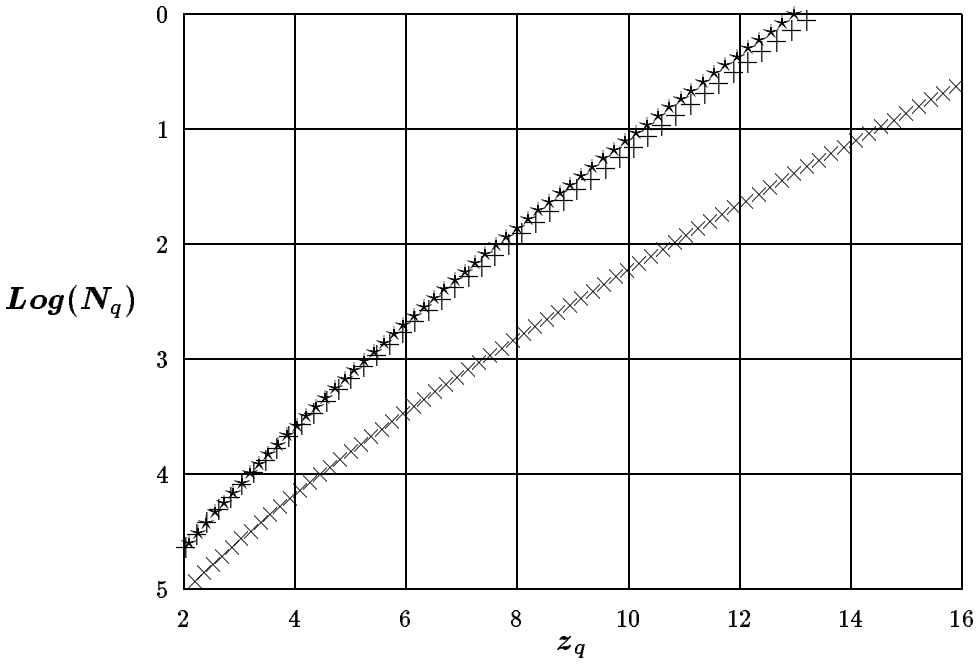

Figure 6